Applied Catalysis A: General 497 (2015) 22–30

Contents lists available at ScienceDirect

Applied Catalysis A: General

journal homepage: www.elsevier.com/locate/apcata

Palladium–bismuth intermetallic and surface-poisoned catalysts for the semi-hydrogenation of 2-methyl-3-butyn-2-ol

Nikolay Cherkasov[a], Alex O. Ibhadon[a,*], Alan J. McCue[b], James A. Anderson[b], Shaun K. Johnston[a]

[a] Catalysis and Reactor Engineering Research Group, Department of Chemistry and School of Biological, Biomedical and Environmental Sciences, University of Hull, Cottingham Road, Hull HU6 7RX, United Kingdom
[b] Surface Chemistry and Catalysis Group, Department of Chemistry, University of Aberdeen, Meston Walk, Old Aberdeen AB24 3UE, United Kingdom

ARTICLE INFO

Article history:
Received 1 December 2014
Received in revised form 4 February 2015
Accepted 20 February 2015
Available online 27 February 2015

Keywords:
Heterogeneous catalysis
Alkynol
2-Methyl-3-butyn-2-ol
Hydrogenation
Semi-hydrogenation
Palladium
Bismuth

ABSTRACT

The effects of poisoning of Pd catalysts with Bi and annealing in a polyol (ethylene glycol) were studied on the semi-hydrogenation of 2-methyl-3-butyn-2-ol (MBY). An increase in the Pd:Bi ratio from 7 to 1 in the Bi-poisoned catalysts decreased the hydrogenation activity due to blocking of active sites, but increased maximum alkene yield from 91.5% for the Pd catalyst to 94–96% for all Bi-poisoned Pd catalysts, by decreasing the adsorption energy of alkene molecules and suppressing the formation of β-hydride phase. Annealing of the catalysts induced the formation of intermetallic phases and decreased its activity due to sintering of the catalytic particles and low activity of intermetallic compounds. Langmuir–Hinshelwood kinetic modelling of the experimental data showed that poisoning of Pd with Bi changed the relative adsorption constants of organic species suggesting ligand effects at high Bi content.

1. Introduction

Semi-hydrogenation or selective hydrogenation reactions aim to transform triple-bonded molecules into double bonded ones, and constitute critical steps in the synthesis of a vast array of fine chemicals including vitamins, fragrances, drugs and many other products with a worldwide production of more than 1000 t a year [1,2]. However, traditional hydrogenation catalysts including supported nanoparticles of Pd and Pt usually lead to low catalyst selectivity. To overcome the problem, the catalysts are usually modified with reversible and irreversible adsorbates which introduce ligand (electronic) effects that change the relative adsorption energies and selectively block the active sites responsible for side-reactions [3,4].

The catalyst modification is performed by surface poisoning and alloying. For example, active sites of Pd in Pd–Ag alloys are isolated, which decreases the rate of oligomerization, while silver induces ligand effects changing the adsorption energies facilitating desorption of alkenes [5,6]. Often, carbon monoxide (a reversible adsorbate) is added to the acetylene feedstock to increase selectivity by competing with alkene molecules for adsorption sites [7,8]. Lindlar catalyst, an industrial standard for semi-hydrogenation, employs lead as an irreversible adsorbate and quinoline as a reversible adsorbate. Metals such as Cu have been extensively studied as irreversible adsorbates [9,10] while sulphur- and nitrogen-containing polymer modifiers combine the functions of reversible and irreversible adsorbates [11,12]. However, the increase in selectivity brought about by modifiers is usually counterbalanced by the decrease in activity [2,10,13], so industrial semi-hydrogenation catalysts should combine an optimal level of catalyst poisoning to improve selectivity while minimising decrease in activity. Moreover, other considerations such as catalyst price, the environmental footprint of catalyst synthesis and the overall economy of the catalytic process should be considered. In this respect, Lindlar catalyst is still the main catalyst used by industry because of its high activity, selectivity and ease of preparation. However, there are a number of problems associated with the use of Lindlar catalysts including the toxicity of lead compounds and that an additional separation step is required when quinoline is used.

In order to address these problems, bimetallic Pd-based catalysts are being studied to improve selectivity and to mitigate environmental problems associated with the use of lead in Lindlar catalyst. Highly selective Pd–Zn alloys were shown to form in

* Corresponding author. Tel.: +44 1723 357241.
E-mail address: a.o.ibhadon@hull.ac.uk (A.O. Ibhadon).

http://dx.doi.org/10.1016/j.apcata.2015.02.038
0926-860X/

Pd/ZnO catalysts during hydrogenation [14–17] while many other bimetallic systems have been studied and theoretically evaluated [4,18]. However, from an industrial point of view, the synthesis of an industrial semi-hydrogenation catalyst should be scalable, hence many catalytic systems that require expensive metallorganic precursors for their synthesis and very carefully controlled reaction conditions cannot compete with Lindlar catalyst. A rather recent trend in catalysis is the study of the intermetallic compounds, which can be defined as electrically conductive compounds of metals, but the most interesting properties for catalytic applications might be precisely defined structural order and electronic properties different from that of initial metals [19]. For example, palladium–gallium intermetallic compounds have been reported to be very selective in acetylene hydrogenation [20]; however, recent data show that Pd_2Ga intermetallic compounds oxidise quickly in liquid-phase hydrogenation even under carefully controlled laboratory conditions due to the high oxygen affinity of Ga [21].

Therefore, in an attempt to identify promising catalysts, considering their performance and the ease of synthesis, we have confined our attention in this study to easily reducible heavy metals. Lead, the adsorbate in Lindlar catalyst, has two neighbours in the periodic table: thallium and bismuth. Palladium-based catalysts modified with either one of these metals showed very high selectivity in hydrodechlorination reactions [22], but considering the extremely high toxicity of thallium, palladium–thallium catalysts cannot be considered as a promising alternative to Lindlar catalyst. In contrast to lead, the toxicity of bismuth is significantly lower [23–25], which makes it a promising catalyst for industrial applications in the semi-hydrogenation in the synthesis of fine chemicals.

Palladium–bismuth systems have been studied in oxidative acetoxylation reactions and Pd_3Bi intermetallic compounds have been found to be the most selective [26,27]. Promotion of Pd with Bi was found to increase the selectivity to the partial oxidation of glucose to gluconic acid [28–30]. Similarly, in hydrogenation reactions, intermetallic compounds of Pd and Bi were identified as promising highly selective catalysts [31–33]. Anderson and co-workers studied a Pd catalyst selectively poisoned with Bi and demonstrated the preferential adsorption of Bi on step sites, which had little effect on 1-hexyne hydrogenation, but decreased the rates of subsequent 1-hexene isomerisation reactions [34,35]. To the best of our knowledge, intermetallic compounds of palladium and bismuth have not been tested in semi-hydrogenation reactions. These catalysts could potentially combine the advantages of Pd–Ga intermetallics with low toxicity and ease of synthesis of bismuth-modified catalysts.

The aim of the study was to investigate the effects of Bi-poisoning and intermetallic formation of Pd catalysts on the semi-hydrogenation of 2-methyl-3-butyn-2-ol (MBY), an important industrial intermediate used in the synthesis of fine chemicals and vitamins [1,36,37].

2. Experimental

2.1. Catalyst preparation

Pd/SiO_2 catalyst with the Pd nominal loading of 5% was prepared by dissolving palladium (II) acetate ($Pd(Oac)_2$, 98%, Aldrich) in the calculated amount of toluene (99%, VWR chemicals) to fill the pores of amorphous fumed silica (Alfa Aesar, BET specific surface area of 200 $m^2\,g^{-1}$). The slurry was dried in a rotary evaporator, calcined in a tube furnace at 400 °C for 2 h and reduced in hydrogen at 150 °C for 1 h. Amorphous silica and high Pd loading were deliberately chosen to allow for analysis by X-ray diffraction.

The catalyst obtained was poisoned with Bi. Pd/SiO_2 catalyst (about 700 mg) was placed into a 50 mL flask and 2% acetic acid (20 mL) in distilled water was added. Then the calculated aliquot of a 20 mM $Bi(NO_3)_3$ solution in 2% acetic acid was added under stirring to obtain the catalysts with Pd/Bi ratios of 1/1, 3/1 and 7/1 assuming that all Bi was reduced from the solution. The dispersion was stirred for 16 h at 80 °C in hydrogen atmosphere. The catalysts were centrifuged, washed with water (2 × 40 mL), acetone (3 × 30 mL), and dried in a rotary evaporator at 80 °C. After cooling of the samples in the rotary evaporator to room temperature, the vacuum pump was turned off, slowly admitting air to the catalyst over a period of about 2 h to passivate the surface. The catalysts were packed into vials and kept under a nitrogen atmosphere to prevent further oxidation. The surface-poisoned catalysts obtained were named Pd_7Bi/SiO_2, Pd_3Bi/SiO_2 and Pd_1Bi/SiO_2 to reflect the nominal Pd:Bi ratio.

Each Bi-poisoned catalyst was annealed in ethylene glycol to induce the formation of intermetallic phases adapting the polyol method [38]. The catalyst (400 mg) was placed into a round-bottom flask and 50.0 mL of ethylene glycol (99%, Fisher Scientific) was added under stirring. Air from the flask was displaced by a flow of nitrogen for 5 min; the slurry was heated, refluxed at 196 °C for 20 min, and cooled in nitrogen flow. The catalysts obtained were centrifuged, washed, passivated as per Bi-poisoned Pd catalysts, and named as $Pd_1Bi(t)/SiO_2$, $Pd_3Bi(t)/SiO_2$ and $Pd_7Bi(t)/SiO_2$.

Unsupported nanoparticles of Pd–Bi intermetallic compounds were obtained using the polyol method annealing Pd and Bi precursors in the presence of polyvinylpyrrolidone (PVP, Sigma–Aldrich) [38]. $Pd(Oac)_2$ (50 mg) and $Bi(NO_3)_3{\cdot}3H_2O$ (the amount was calculated to obtain Pd:Bi molar ratios of 1:1 and 1:2) were dissolved in 75 mL of ethylene glycol under sonication, PVP (250 mg) was slowly added under stirring. After 30 min, $NaBH_4$ (300 mg, 98%, Sigma–Aldrich) was added and the solution was heated and refluxed under nitrogen flow for 20 min. When the slurry was cooled, the dispersion was diluted with 50 mL methanol, centrifuged, washed with water (2 × 30 mL), methanol (2 × 30 mL), acetone (2 × 30 mL) and left in 20 mL of acetone. The dispersion obtained was sonicated for 10 min and 15 mL were used to impregnate silica (800 mg) giving raise to $PdBi(im)/SiO_2$ and $PdBi_2(im)/SiO_2$ catalysts.

Lindlar catalyst (Pd poisoned with Pb supported on $CaCO_3$) was purchased from Aldrich and used as received without the addition of quinoline.

2.2. Characterisation

Powder X-ray diffraction (PXRD) measurements were performed using an Empyrean X-ray diffractometer equipped with a monochromatic Kα-Cu X-ray source and a PIXcel linear detector. The scanning was performed in 2θ range of 20–85°, step length 0.0390°, and step time 25 min. Silica-supported catalysts were packed into conventional powder holders, while the dispersion of the intermetallic nanoparticles in acetone was dropwise added on a silicon zero-background sample holder.

Scanning electron microscopy (SEM) study was performed on a Zeiss EVO 60 instrument equipped with energy-dispersive X-ray spectrometer (EDX) Oxford Instruments Inca System 350 under the pressure of 10^{-2} Pa and electron acceleration voltage of 20 kV. Catalyst powder was applied on carbon adhesive mats and carbon-coated before the study.

Transmission electron microscopy (TEM) study was performed using a Jeol 2010 instrument equipped with an energy-dispersive X-ray spectrometer (EDX) produced by Oxford Instruments. For the study, the materials were dispersed in ethanol under sonication and a few droplets of the dispersion were applied on carbon-coated copper grids. TEM study was performed from 5–8 regions for every sample to obtain representative data.

Elemental analysis was performed using a Perkin Elmer Optima 5300DV emission inductively coupled plasma spectrometer. The

samples were weighed and dissolved in the mixture of HF (1 mL), HCl (1 mL) and HNO_3 (3 mL) in Teflon digestion vessels using a microwave digestion system (CEM MARS Xpress Plus). After heating at 200 °C for 10 min and cooling, saturated boric acid (5 mL) was added to each and then sealed and reheated at 180 °C for 10 min, to complex excess HF before dilution and analysis.

Carbon monoxide uptake and temperature-programmed reduction (TPR) was performed for selected catalysts using a CE Instruments TPDRO 1100 equipped with a TCD detector. Sample was placed in a quartz reactor tube and reduced in a flow of 5% H_2/N_2 (40 mL min^{-1}). During the reduction step, the sample was heated from room temperature to 100 °C at 10 °C min^{-1} and held at that temperature for 1 h. The sample was then cooled to 35 °C before CO was pulsed (0.285 mL loop size) into a He flow until constant peak area were obtained (*i.e.*, no further uptake was apparent). Turn-over frequency (TOF) was calculated using an average reaction rate ($A_{average}$) up to about 80% MBY conversion assuming a Pd:CO ratio of 1.5 since bridging species generally contribute significantly to the observed uptake for Pd samples [34].

2.3. Catalyst testing

A freshly prepared catalyst was transferred into a double-neck flask, containing hexane (15 mL, 98%, Fisher Scientific) and butanol-1 (15 μL, 99%, Fisher Chemical) as an internal standard. The solution was degassed by bubbling nitrogen (99.999%, CK gas) for 20 min while stirring at 1100 rpm. Afterwards, the system was flushed twice with hydrogen (99.999%, CK gas), evacuating until the residual pressure reached about 40 mbar following by filling with hydrogen to ambient pressure. The system was left for 30 min under stirring at 50 °C to achieve equilibrium and to ensure the absence of leaks, which was done by monitoring the hydrogen level using a 25 mL gas burette. The reaction flask was kept in a water bath at 50 ± 0.1 °C. To test the most active catalysts (Pd/SiO_2, Lindlar, Pd_7Bi/SiO_2, $Pd_7Bi(t)/SiO_2$), 5 mg of the catalyst was added; 40 mg was used for medium-activity catalysts (Pd_3Bi/SiO_2, $Pd_3Bi(t)/SiO_2$) and 100–250 mg for other catalysts to perform the reaction within 1–4 h.

Hydrogenation reaction was started by injecting a 25% MBY (260 mg, 98%, Sigma–Aldrich) solution in hexane. During the reaction, aliquots (80 μL) were extracted with the increased sampling rate close to 100% MBY conversion (monitored using hydrogen consumption). The extracted samples were analysed on a Varian 430 gas chromatograph (GC) fitted with a flame ionisation detector, an autosampler and a 30 m Stabiwax capillary column. The absence of pore mass transfer limitations was confirmed calculating Weisz–Prater number for MBY and dissolved hydrogen, as described by Vannice [39]. The numbers for the fastest Pd/SiO_2 catalyst were several orders of magnitude lower than the boundary value of 6 (0.001 and 0.008 for hydrogen and MBY, respectively), which shows that pore transfer limitations do not apply. The absence of external mass transfer limitations was confirmed studying the effect of stirring speed on the hydrogen consumption rate, which did not increase at the stirring speed above 500 rpm.

2.4. Kinetic modelling

Fig. 1 shows the scheme of the MBY hydrogenation, where along with the reaction of interest, MBY to 2-methyl-3-buten-2-ol (MBE) hydrogenation, further hydrogenation to 2-methyl-2-butanol (MBA) and direct full hydrogenation of MBY to MBA are possible [17].

The Langmuir–Hinshelwood model was adopted from the works of Singh and Vannice [40] and Duca et al. [41], considering quasi-equilibrium competitive adsorption of organic and hydrogen species on the catalyst surface followed by rate-determining

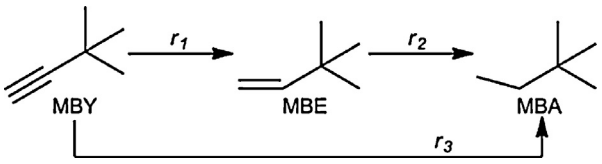

Fig. 1. Scheme of hydrogenation reactions of MBY.

steps between the adsorbed species. Only MBY, MBE and MBA were included into the model, because no other products were identified and the carbon balance was always 100 ± 2% (Fig. 2c). The hydrogen adsorption constant was considered to be low under the experimental conditions, and relative (rather than absolute) adsorption constants $Q_1 = K_{MBE}/K_{MBY}$, $Q_2 = K_{MBA}/K_{MBY}$ were used due to strong adsorption of organic species [41]. The reaction rates obtained (as designated in Fig. 1) are presented in Eqs. (1)–(3), where k_1^*, k_2^*, k_3^* are the apparent rate constants, C_{MBY}, C_{MBE}, C_{MBA} are concentrations of MBY, MBE and MBA, respectively.

$$r_1 = \frac{k_1^* C_{MBY}}{(Q_1 C_{MBE1} + C_{MBY} + Q_2 C_{MBA})^2} \quad (1)$$

$$r_2 = \frac{k_2^* C_{MBE}}{(Q_1 C_{MBE} + C_{MBY} + Q_2 C_{MBA})^2} \quad (2)$$

$$r_3 = \frac{k_3^* C_{MBY}}{(Q_1 C_{MBE} + C_{MBY} + Q_2 C_{MBA})^2} \quad (3)$$

The reaction rates presented were integrated in Matlab using an ode15s solver which is efficient for stiff systems of differential equations. The model parameters were optimised using the Levenberg–Marquardt algorithm [42] to minimise the objective function S presented in Eq. (4), where C_{exp} and $C_{modelled}$ are experimental and modelled concentrations, ω_i are statistical weights. The statistical weights were calculated using experimental standard deviations $\sigma_{exp,i}$ determined for the analytical technique used, which were 2% of the determined value or 0.3 mol m^{-3}, whichever is larger [43]. Confidence intervals (90% probability) of the model parameters were determined using the Monte-Carlo method, which takes into account the covariation of the model parameters [44].

$$S = \sum_i \omega_i (C_{exp,i} - C_{mod,i})^2; \quad \omega_i = \frac{1}{\sigma_{exp,i}^2}. \quad (4)$$

3. Results and discussion

3.1. Hydrogenation on Pd/SiO_2 and Lindlar catalysts

Fig. 2a and b presents a comparison of MBY hydrogenation using monometallic palladium (Pd/SiO_2) and Lindlar catalysts. The concentration profiles of both catalysts were similar and consisted of two consecutive stages: hydrogenation of MBY to MBE and MBE to MBA (Fig. 1). In the presence of MBY, the over-hydrogenation to MBA was comparatively low, which is traditionally related to the strong adsorption of alkyne molecules on a Pd surface [2,4,45,46]. Carbon balance for these systems (Fig. 2c) was 100 ± 2%, showing that products other than MBY, MBE and MBA were not formed in significant quantities.

However, the behaviour of the catalysts was not identical. The difference was most obvious in the derivative plots which show the apparent reaction rates (Fig. 2a and b, top). The Pd/SiO_2 catalyst showed a higher absolute reaction rates compared to the Lindlar catalyst. These effects have also been observed by other authors for various substrate molecules [13,34,47,48] and can be explained by a combination of two factors. Firstly, catalyst support had a significant effect on the dimensions of Pd nanoparticles formed:

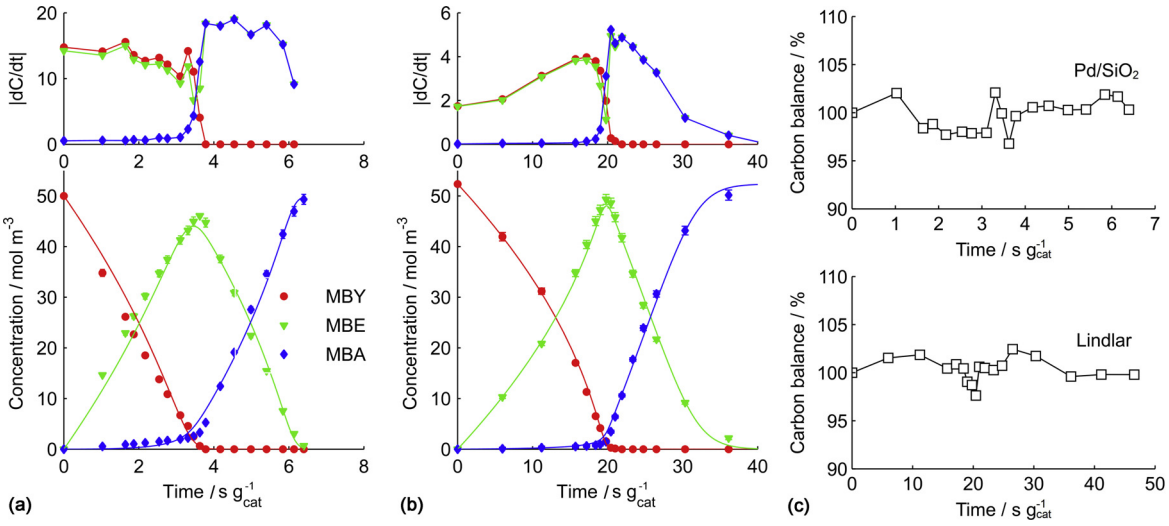

Fig. 2. Concentration profiles of MBY hydrogenation on the (a) Pd/SiO_2 and (b) Lindlar catalysts with dots representing experimental data and lines – Langmuir–Hinshelwood model (see Section 3.4). Corresponding derivative plots above the concentration profiles show the apparent reaction rates (the unit is mol m^{-3} s^{-1} g_{cat}^{-1}). (c) Carbon balances for hydrogenation on Pd/SiO_2 and Lindlar catalysts.

high-surface area silica (S_{BET} 200 m^2 g^{-1}) stabilised Pd nanoparticles 7.4 ± 2.2 nm in diameter according to the TEM study (Fig. 3a and b), while Pd nanoparticles on $CaCO_3$ (S_{BET} 3.3 m^2 g^{-1}) formed agglomerates up to 0.1–1 μm (Fig. 3c). Secondly, poisoning with Pb further decreased the activity of Pd catalysts due to blocking of some Pd active sites [13,34].

Another notable difference between the catalysts was in the temporal behaviour of MBY and MBE hydrogenation rates, which were almost constant in the Pd/SiO_2 catalyst (Fig. 2a, top). Conversely, in the Lindlar catalyst, the rates accelerated near the point of maximum MBE yield (Fig. 2b, top), demonstrating the suppression of the alkene adsorption on Pd surface in the presence of Pb due to ligand effects [3]. More importantly, MBA formation rate at the initial reaction stages was significant in the Pd/SiO_2 catalyst leading to a lower maximum MBE yield of 91.4% in comparison to 94.5% for the Lindlar catalyst. As a result, these catalysts demonstrate a compromise between higher activity that can be achieved on monometallic Pd catalysts (Pd/SiO_2) and higher selectivity demonstrated by the Lindlar catalyst [21,49].

3.2. Hydrogenation on Bi-poisoned Pd/SiO_2 catalysts

In order to find more environmentally benign semi-hydrogenation catalysts while keeping the synthesis procedure simple, Bi was selected as a poisoning agent. A number of detailed studies showed that Bi preferentially adsorbs on step and edge sites of Pt and terrace sites are occupied afterwards [50–52]. Furthermore, Anderson et al. [34] confirmed using infrared (IR) spectroscopy that Bi poisons preferentially step and edge sited of Pd catalysts, the sites that preferentially over-hydrogenate MBY as found by Crespo-Quesada et al. [53]. Hence, the rate of MBE hydrogenation was expected to decrease considerably because of the incorporation of Bi, so a series of Bi-poisoned Pd catalysts were prepared from the same batch of Pd/SiO_2 catalyst.

TEM study of the catalysts showed that the diameter of the metal nanoparticles did not change significantly on the introduction of Bi. EDX study of individual particles showed the presence of Pd and Bi, which confirms adsorption of Bi on Pd nanoparticles and no purely Bi particles were identified. IR study of chemisorbed CO on the catalysts was attempted in the transmission and diffused reflectance modes; however, the absorbance was very high to allow for spectra acquisition. Nevertheless, thermodynamic preference of Bi atoms to adsorb on step and edge sites of platinum-group metals, which was shown both experimentally and theoretically [4,34,50,51], the same method of Bi introduction used by Anderson et al. [34] and in the current work confirms that Bi was adsorbed on step and edge sites.

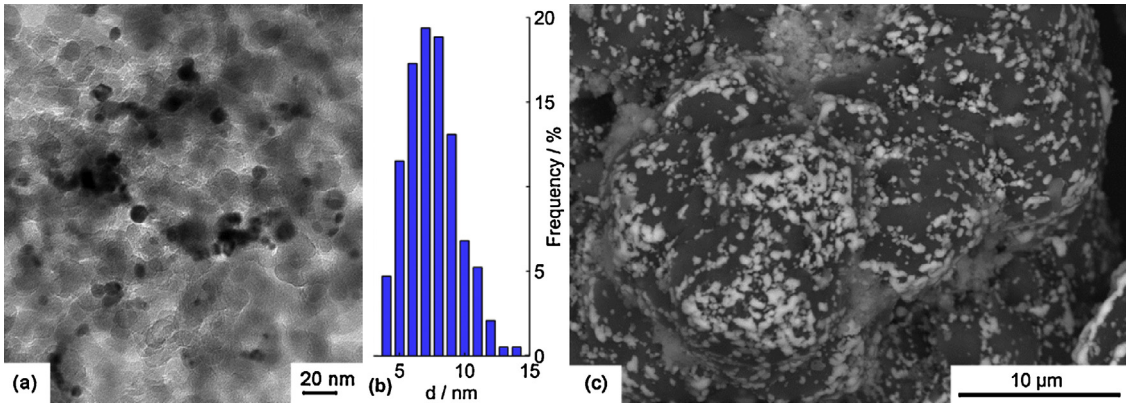

Fig. 3. Representative (a) TEM image of Pd/SiO_2 catalyst and (b) corresponding Pd nanoparticle size distribution. (c) SEM image of the Lindlar catalyst in the backscattered electron mode which highlights Pd–Pb particles.

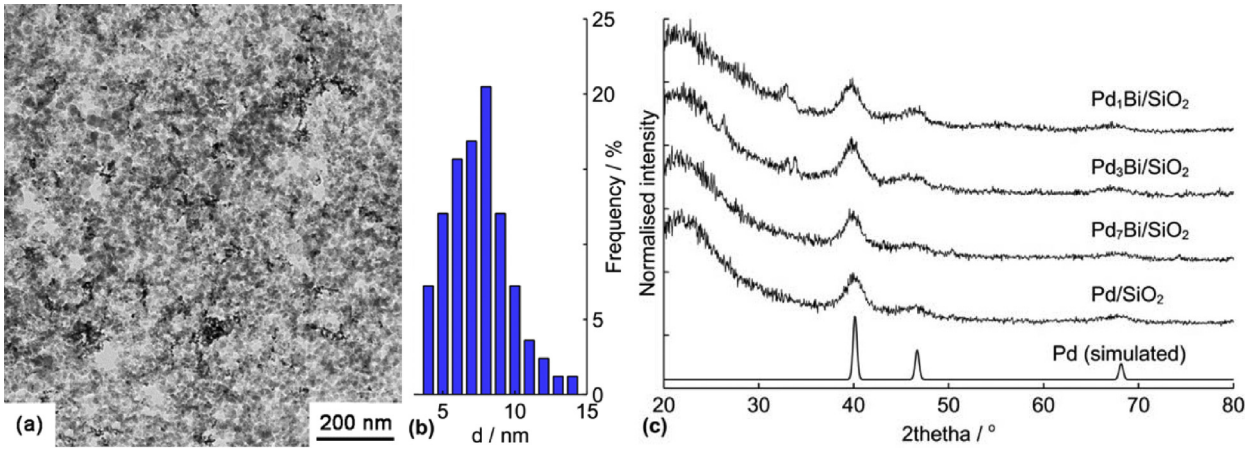

Fig. 4. (a) Representative TEM image of Pd_1Bi/SiO_2 catalyst and (b) corresponding particle size distribution. (c) PXRD patterns of initial and Bi-poisoned catalysts.

Table 1
Elemental analysis of the catalysts studied.

Catalyst	Pd (wt%)	Bi (wt%)	Pd/Bi (mol)
Pd/SiO_2	5.11	0	–
Lindlar	4.22	0.69 (Pb)	–
Pd_7Bi/SiO_2	4.74	1.31	7.13
Pd_3Bi/SiO_2	4.51	2.95	3.01
Pd_1Bi/SiO_2	4.51	5.03	1.77
$Pd_7Bi(t)/SiO_2$	4.77	1.30	7.22
$Pd_3Bi(t)/SiO_2$	5.60	2.89	3.14
$Pd_1Bi(t)/SiO_2$	4.52	4.71	1.89
$PdBi(im)/SiO_2$	0.92	1.68	1.08
$PdBi_2(im)/SiO_2$	0.68	2.52	0.53

The dimensions of the nanoparticles in the Pd_1Bi/SiO_2 catalyst, 7.2 ± 2.1 nm (Fig. 4a and b), were similar to that found in the Pd/SiO_2 catalyst. PXRD study (Fig. 4c) showed very similar patterns with the reflexes attributed to Pd nanoparticles of 5.0 ± 0.2 nm in diameter according to Scherrer equation. Interestingly, Bi content (5.0%) observed in Pd_1Bi/SiO_2 (Table 1) was much higher than can be expected based only on the surface poisoning, because only 1.26% of Bi was needed to achieve monolayer coverage of surface Pd sites. This indicates either (a) the deposition of Bi nanoparticles on the support material, or (b) multilayer adsorption on the surface of Pd particles. Multilayer adsorption on the Pd surface should have increased the average particle diameter from 7.4 to 9.6 nm, which is not supported by TEM studies (Fig. 4b). As such, deposition of Bi on the support material is likely, but if Bi particles of 5 nm or larger in diameter were formed they should have been apparent from PXRD measurements due to very high intensity of Bi (intensity of Bi reflexes is 5 times as high as that for Pd). Given that PXRD patterns show no evidence of reflections associated with Bi, any monometallic Bi particles are expected to be small in size. This may be supported by a small shift in the particle size distribution observed by TEM (Figs. 3b and 4b). After Bi addition, there is a small increase in the number of particles observed that are smaller than 4 nm in size, although, the change is small and should not be considered as conclusive. Although the formation of Bi nanoparticles cannot be entirely ruled out, we believe that Bi adsorbed on Pd nanoparticles, preferentially on edge sites as demonstrated by DFT calculations, IR-studies for Pd–Bi and electrochemical studies Pt–Bi system [4,34,50,51].

Fig. 5 shows the concentration profiles of MBY hydrogenation on Bi-poisoned Pd catalysts. The derivative plots (Fig. 5, top) demonstrate that with the increase in Bi poisoning, the reaction rates decreased by almost 50 times comparing Pd_7Bi/SiO_2 and Pd_1Bi/SiO_2 catalysts. More importantly, for all Bi poisoned catalysts, MBA formation rate at the initial reaction stages were low, allowing maximum MBE yield of 94–96% (similar to the Lindlar catalyst). The apparent reaction rates on the Bi-poisoned catalysts decreased compared to Pd/SiO_2, which was expected considering that the number of active sites decreased with the Bi poisoning. Moreover, the poisoning had different effect on the ratio of the apparent MBY and MBE consumption rates. The derivative plots in Fig. 5a–c (top) show that on Pd_7Bi/SiO_2, the apparent rate of MBE hydrogenation was higher than that of MBY, while on Pd_1Bi/SiO_2, MBE hydrogenation was almost suppressed.

3.3. Hydrogenation on the annealed Bi-poisoned Pd/SiO_2 catalysts

Intermetallic compounds are usually obtained by melting metals in an inert atmosphere [54–57], however very high temperatures are required (about 1000–2000 °C) resulting in the particles showing low activity due to low dispersity [20,21]. A polyol method overcomes this problem and implies the annealing of metal precursors at much lower temperatures (200–300 °C) in polyol solvents such as glycerol, ethylene or tetraethylene glycols, which provide reducing environment, facilitate fusion of metal nanoparticles and act as capping agents [38,58,59].

Palladium and bismuth form several intermetallic phases that are stable below 200 °C with the chemical formulae $PdBi_2$, PdBi, Pd_2Pd_5, Pd_3Bi [55–57]; and recent data show that Pd does not alloy with Bi [56]. According to Heise et al. [58], intermetallic phases of Pd and Bi are formed at 170–240 °C on microwave-assisted polyol synthesis, while similar PtBi intermetallic compounds form on brief annealing of Pt–Bi nanoparticles at 220 °C [38]. Because intermetallic Pd–Bi compounds were demonstrated to be promising catalysts for various oxidation reactions [26–30], the Bi-poisoned Pd catalysts obtained were refluxed in ethylene glycol to induce the formation of intermetallic compounds. PXRD data (Fig. 6a) show that on annealing, intermetallic compound Pd_5Bi_2 was formed in the $Pd_1Bi(t)/SiO_2$ catalyst. A TEM study of the annealed catalysts showed that metal nanoparticles formed chain-like agglomerates (Fig. 6b and c) and led to an increase in nanoparticles dimensions, being 9.9 ± 3.6 nm for $Pd_7Bi(t)/SiO_2$ catalyst, and 15 ± 8 nm for $Pd_3Bi(t)/SiO_2$ and $Pd_1Bi(t)/SiO_2$ catalysts. EDX study of individual particles confirmed the presence of Pd and Bi. So the significant increase in the nanoparticle dimensions observed for the poisoned catalysts was likely caused by the increased mobility due to introduction of low-melting Bi (bulk phase melting point is 271 °C [55]).

The concentration profiles of MBY hydrogenation using the annealed catalysts are presented in Fig. 7a–c. Similar to the

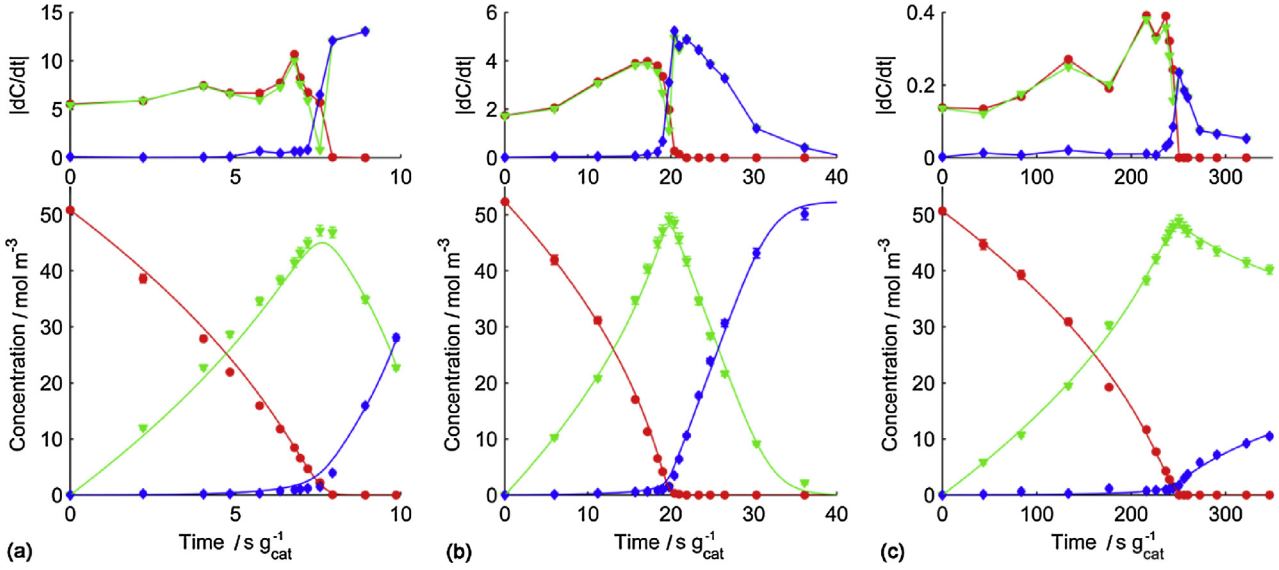

Fig. 5. Concentration profiles of MBY hydrogenation on (a) Pd_7Bi/SiO_2, (b) Pd_3Bi/SiO_2, (c) Pd_1Bi/SiO_2 catalysts with dots representing experimental data (the same designations as in Fig. 2) and lines – Langmuir–Hinshelwood model (see Section 3.4). Corresponding derivative plots above the concentration profiles show the apparent reaction rates (the unit is mol m^{-3} s^{-1} g_{cat}^{-1}).

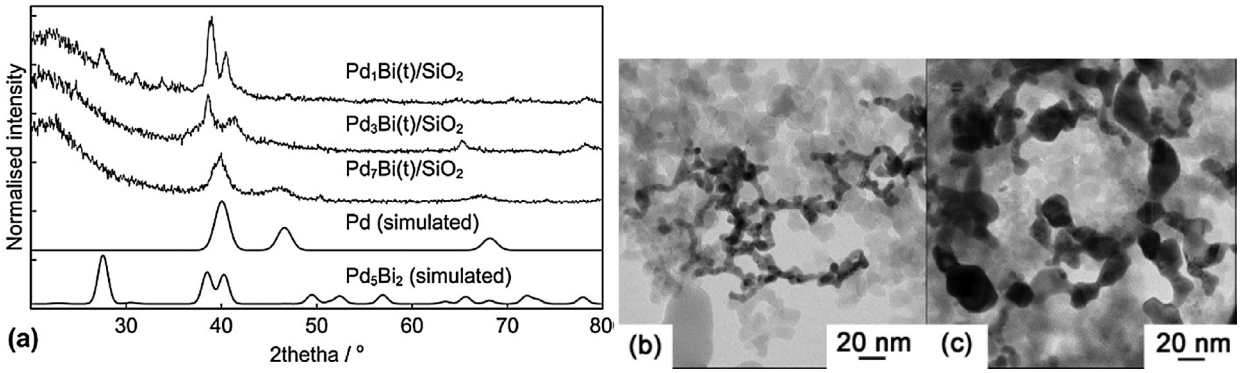

Fig. 6. (a) PXRD patterns of Bi-poisoned Pd catalysts annealed in ethylene glycol at 196 °C for 20 min. Representative TEM microphotographs of the (b) $Pd_7Bi(t)/SiO_2$ and (c) $Pd_3Bi(t)/SiO_2$ catalysts.

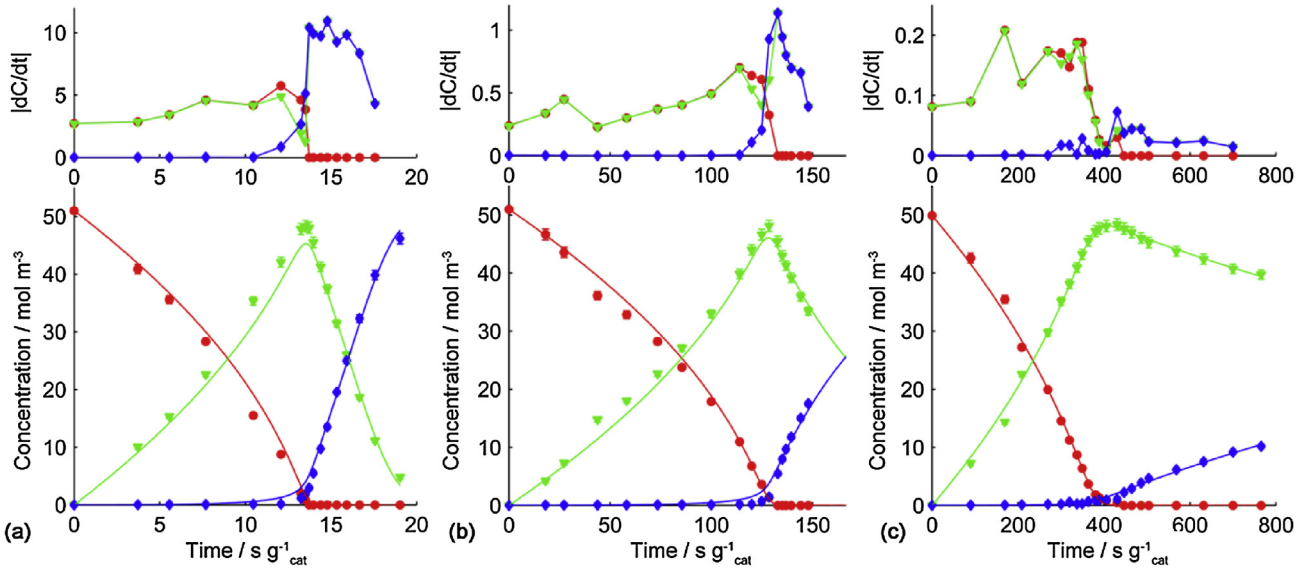

Fig. 7. Concentration profiles of MBY hydrogenation on (a) $Pd_7Bi(t)/SiO_2$, (b) $Pd_3Bi(t)/SiO_2$ and (c) $Pd_1Bi(t)/SiO_2$ catalysts annealed in ethylene glycol at 196 °C for 20 min with dots representing experimental data (the same designations as in Fig. 2) and lines – Langmuir–Hinshelwood model (see Section 3.4). Corresponding derivative plots above the concentration profiles show the apparent reaction rates (the unit is mol m^{-3} s^{-1} g_{cat}^{-1}).

Table 2
CO chemisorption and TPR data, average reaction rate per mol of Pd ($A_{average}$) and TOF.

	$A_{average}$ (min^{-1})	CO uptake ($\mu mol\,g^{-1}$)	TOF (s^{-1})	H_2 release[a] ($\mu mol\,g^{-1}$)
Pd/SiO_2	35	60.3	3.03	254
$Pd_7Bi(t)/SiO_2$	7.1	23.9	1.56	62.3
Pd_1Bi/SiO_2	0.41	6.6	0.32	n.d.
$PdBi(im)/SiO_2$	0.12	n.d.	–	n.d.

n.d. = not detected.
[a] Release of hydrogen as a result of palladium hydride decomposition during the TPR.

initial Bi-poisoned Pd catalysts, the activity of the annealed catalysts decreased at higher Bi content, being 2–3 times less active than the corresponding Bi-poisoned catalysts, which was expected considering the observed increase in the dimensions of the nanoparticles. Furthermore, the relative apparent reaction rates of MBY and MBE consumption for the annealed catalysts changed with Bi poisoning. For the $Pd_7Bi(t)/SiO_2$ and $Pd_3Bi(t)/SiO_2$ catalysts, MBE consumption rate was higher than the MBY consumption, while the intermetallic-containing $Pd_1Bi(t)/SiO_2$ catalyst showed very low apparent rate of MBE consumption. However, in comparison with the Pd/SiO_2 catalyst, the apparent MBY consumption rate for the $Pd_1Bi(t)/SiO_2$ catalyst was more than 100 times slower (derivative plots in Figs. 2a and 7c).

The synthesis of intermetallic catalysts, $PdBi_2(im)/SiO_2$ and $PdBi(im)/SiO_2$ was attempted using the polyol method leading to the formation of a mixture of several intermetallic phases ($PdBi_2$, PdBi, and Pd_5Bi_2). Interestingly, the $PdBi_2(im)/SiO_2$ catalyst showed a very unusual behaviour for Pd based catalysts, preferentially forming MBA (selectivity of 75%), rather than MBE, even at low MBY conversion (Fig. S1 in the Supplementary Data). However, the observed activity of the catalysts was 500–2000 times lower in comparison to Pd/SiO_2 hence little promise of hydrogenation application.

3.4. Kinetic modelling

The effects of Bi poisoning and annealing was compared studying the apparent reaction rate and adsorption constants derived by kinetic modelling as described in Section 2.4. For better understanding of the model parameters, Eqs. (1) and (2) can be simplified by neglecting MBA and MBY concentrations during the predominant MBY and MBE hydrogenation stages giving rise to Eqs. (5) and (6). High values of the apparent rate constants are responsible for the increase in the corresponding reaction rates, while high relative adsorption constants Q_1 and ($Q_3 = Q_2/Q_1$) decrease the reaction rates due to saturation of the active sites with the reacting molecules and displacement of hydrogen species from the catalyst surface.

$$r_1 \approx \frac{k_1^* C_{MBY}}{(C_{MBY} + Q_1 C_{MBE1})^2} \quad (5)$$

$$r_2 \approx \frac{k_2^* C_{MBE} Q_1^{-2}}{(C_{MBE} + Q_2/Q_1 C_{MBA})^2} \quad (6)$$

The solid lines in Figs. 2, 5 and 7 show the modelled concentration profiles, which are in good agreement with the experimental data. The resulting kinetic parameters obtained by the fitting are presented in Fig. 8. The apparent rate constant k_1 (Fig. 8a) of the MBY to MBE hydrogenation reaction decreased with the increasing Bi content for Bi-poisoned and the annealed Bi-poisoned catalysts. The annealing step decreased the k_1 constant further by 2.5–1.5 times possibly due to the sintering of the nanoparticles as observed by TEM. The apparent rate constant k_2 (Fig. 8b) of MBE to MBA hydrogenation changed similarly to k_1 constant, decreasing for the catalysts with higher Bi content and for the annealed catalysts. Moreover, the k_2 constant was very low for the $Pd_1Bi(t)/SiO_2$ catalyst, showing almost full suppression of the MBE hydrogenation rate. The rate constant k_3 of direct MBY to MBA hydrogenation (Fig. 8c) was at least one order of magnitude lower than the k_2 constant with very wide confidence intervals. Very low values of k_3 show that the direct MBY over-hydrogenation rate was very low, while wide confidence intervals show that very similar concentration profiles can be modelled with a wide range of k_3 parameter values. As a result, MBY hydrogenation on the studied catalysts can be accurately modelled considering only two stepwise hydrogenation stages, not taking into account the direct over-hydrogenation stage.

The relative adsorption constants obtained are of more interest because many theoretical works have shown that adsorption factors play an important role in improving semi-hydrogenation selectivity of Pd-based bimetallic catalysts [3,4,14,60]. The relative adsorption constant Q_1 (Fig. 8d), was similar for all studied catalysts, showing that MBE adsorption constant was 5–15 times lower than the adsorption constant of MBY. As a result, the reaction rates accelerated at low MBY concentrations (Eq. (5)), because a higher fraction of the catalyst surface was free to adsorb hydrogen and MBE species [41]. Interestingly, undoped Pd/SiO_2 catalyst showed the highest value of Q_1 constant, and as a result, the lowest acceleration of the reaction rates at high MBY conversion (Fig. 2) and the lowest MBE selectivity.

In contrast, Q_2 and Q_3 constants, which show the ratio of MBA to MBY and MBA to MBE adsorption constants, respectively, significantly increased at high Bi poisoning (Fig. 8e and f). For the catalysts Pd_1Bi/SiO_2, $Pd_3Bi(t)/SiO_2$ and $Pd_1Bi(t)/SiO_2$, Q_3 value was higher than 1, decreasing the MBE hydrogenation rate as shown in Eq. (6) in the presence of MBA. The intermetallic $PdBi(im)/SiO_2$ had a Q_3 value higher than 100, suggesting that once some MBA was formed as a result of MBE hydrogenation, it blocked the catalyst surface and suppressed further MBE hydrogenation (Fig. 7c).

Fig. 9a shows the correlation between the apparent rate constants k_1 and k_2, which is linear for almost all the catalysts except $PdBi_2(im)/SiO_2$, *i.e.* Bi poisoning decreased both k_1 and k_2 constants almost to the same extent. Hence, the observed change in the relative apparent reaction rates of MBE and MBY consumption for different Bi-poisoned and annealed catalysts can be explained by the change of adsorption constants. For example, Q_1 is squared in Eq. (6), showing very high impact of small variations in the relative adsorption constants on the reaction rates. More surprising is the correlation of Q_2 with the change of k_1 constant (Fig. 9b). The relative adsorption constant Q_2 was almost identical for Pd/SiO_2, Lindlar and the catalysts with low Bi content. For the catalysts Pd_1Bi/SiO_2, $Pd_1Bi(t)/SiO_2$, and intermetallic-containing catalysts, the Q_2 constant increased with the decrease in k_1 constant, which suggests strong ligand effects of Bi on Pd nanoparticles.

To test the possibility of strong ligand effects of Bi on Pd particles, CO chemisorption studies were performed for the selected catalysts to compare the average MBY consumption rates normalised per mole of Pd and per active site (Table 2). The absolute reaction rate decreased by almost 85 times compared Pd/SiO_2 and Pd_1Bi/SiO_2 catalysts, while CO total uptake decreased only by about 10 times. It

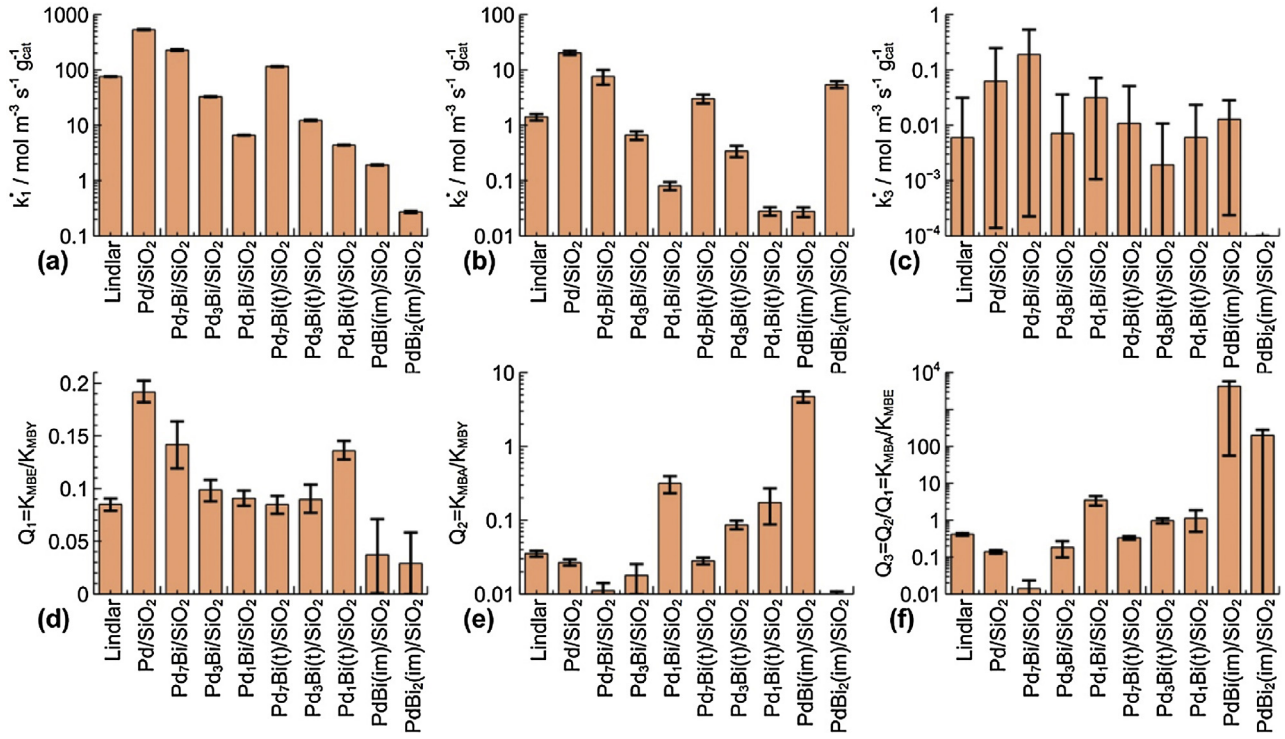

Fig. 8. Langmuir–Hinshelwood model parameters obtained by fitting the experimental data with 90% confidence intervals calculated using the Monte-Carlo method [44].

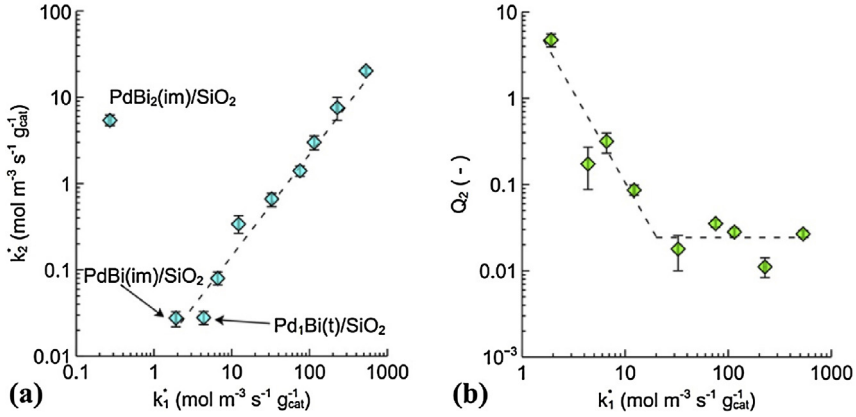

Fig. 9. The correlation between (a) the apparent rate constants k_1 and k_2, and (b) k_1 and Q_2 for all studied catalysts.

shows that the TOF for these catalysts decreased by almost an order of magnitude due to the introduction of Bi. So significant change in TOF indicates ligand effects of Bi on Pd, which led to the change in the hydrogen dissociative adsorption energy – the effect demonstrated for Pd, Pt, Ni-based bimetallic systems by density functional theory calculations [61,62].

Interestingly, TPR data (Table 1) showed that Bi-poisoning has a dramatic effect on the formation of palladium hydride, which decreased by 75% comparing Pd/SiO_2 and $Pd_7Bi(t)/SiO_2$ catalysts. For gas-phase hydrogenation, the formation of sub-surface β-hydride phase was identified as one of the reasons for non-selective hydrogenation [63,64]. A study for Lindlar catalyst, showed that in liquid-phase hydrogenation the poisoning with lead decreased the hydride phase formation [65]. Similarly, the hydrogen consumption data obtained in this work for Bi-poisoned catalysts suggest that Bi suppresses the formation of hydride phase, which, along with the poisoning of edge sites, can be a reason for increased selectivity of Bi-poisoned catalysts.

4. Conclusions

Bi-poisoned Pd catalysts and annealed Bi-poisoned Pd catalysts were compared in the liquid-phase semi-hydrogenation of 2-methyl-3-butyn-2-ol. The poisoning of Pd with Bi increased the maximum alkene yield from 91.5% for Pd/SiO_2 to 94–96% for Bi-poisoned catalysts, which is comparable to the current industrial standard – Lindlar catalyst (94.5%). At a lower Bi content (Pd:Bi ratio above 3) the increased alkene selectivity and decreased activity is likely associated with the adsorption of Bi on the low-selective step and edge sites of Pd nanoparticles [4,34,50,51,53]. At higher Bi content in addition to blocking non-selective Pd sites, Bi induced strong ligand effects and significantly decreased adsorption energy of alkene species. The annealing in ethylene glycol at 196 °C led to the sintering of nanoparticles and induced the formation of Pd_5Bi_2 intermetallic compound, which demonstrated MBY hydrogenation activity about 2 orders of magnitude lower than the Pd catalyst and almost completely suppressed the

alkene hydrogenation rate. Other intermetallic compounds were even less active. However, increasing Bi content and annealing notably increased the adsorption constant of alkane molecules, suppressing alkene hydrogenation. Therefore, results from his study suggest that intermetallic Pd–Bi compounds cannot be considered as promising catalysts for hydrogenation due to very low activity and high price. However, Bi-poisoned Pd catalysts combine the ease of preparation, high activity and alkene selectivity comparable to that of Lindlar catalyst. An important advantage of Pd–Bi catalyst is significantly lower toxicity of Bi in compared to Pb.

Acknowledgements

Authors are grateful to Dr. C. Wiles, Professor P. Fletcher and Professor B. Binks for the access to their equipment and to the EU for an FP7 Grant for the MAPSYN Project (MAPSYN.eu No. CP-IP 309376).

Appendix A. Supplementary data

Supplementary data associated with this article can be found, in the online version, at http://dx.doi.org/10.1016/j.apcata.2015.02.038.

References

[1] W. Bonrath, J. Medlock, J. Schutz, B. Wüstenberg, T. Netscher, in: I. Karame (Ed.), Hydrogenation, InTech, Rijeka, 2012, pp. 69–90.
[2] Á. Molnár, A. Sárkány, M. Varga, J. Mol. Catal. A: Chem. 173 (2001) 185–221.
[3] M. García-Mota, J. Gómez-Díaz, G. Novell-Leruth, C. Vargas-Fuentes, L. Bellarosa, B. Bridier, J. Pérez-Ramírez, N. López, Theor. Chem. Acc. 128 (2011) 663–673.
[4] N. López, C. Vargas-Fuentes, Chem. Commun. 48 (2012) 1379–1391.
[5] N.A. Khan, S. Shaikhutdinov, H.J. Freund, Catal. Lett. 108 (2006) 159–164.
[6] A. Pachulski, R. Schödel, P. Claus, Appl. Catal. A: Gen. 445–446 (2012) 107–120.
[7] J. Silvestre-Albero, G. Rupprechter, H. Freund, J. Catal. 240 (2006) 58–65.
[8] M. García-Mota, B. Bridier, J. Pérez-Ramírez, N. López, J. Catal. 273 (2010) 92–102.
[9] M.P. Spee, J. Boersma, M.D. Meijer, M.Q. Slagt, G. van Koten, J.W. Geus, J. Org. Chem. 66 (2001) 1647–1656.
[10] T.A. Nijhuis, G. van Koten, J.A. Moulijn, Appl. Catal. A: Gen. 238 (2003) 259–271.
[11] T. Mitsudome, Y. Takahashi, S. Ichikawa, T. Mizugaki, K. Jitsukawa, K. Kaneda, Angew. Chem. 52 (2013) 1481–1485.
[12] N.V. Semagina, A.V. Bykov, E.M. Sulman, V.G. Matveeva, S.N. Sidorov, L.V. Dubrovina, P.M. Valetsky, O.I. Kiselyova, A.R. Khokhlov, B. Stein, L.M. Bronstein, J. Mol. Catal. A: Chem. 208 (2004) 273–284.
[13] J.G. Ulan, E. Kuo, W.F. Maier, J. Org. Chem. 52 (1987) 3126–3132.
[14] M.W. Tew, H. Emerich, J.A. van Bokhoven, J. Phys. Chem. C 115 (2011) 8457–8465.
[15] L.N. Protasova, E.V. Rebrov, K.L. Choy, S.Y. Pung, V. Engels, M. Cabaj, A.E.H. Wheatley, J.C. Schouten, Catal. Sci. Technol. 1 (2011) 768–777.
[16] E.V. Rebrov, A. Berenguer-Murcia, H.E. Skelton, B.F.G. Johnson, A.E.H. Wheatley, J.C. Schouten, Lab Chip 9 (2009) 503–506.
[17] E.V. Rebrov, E.A. Klinger, A. Berenguer-Murcia, E.M. Sulman, J.C. Schouten, Org. Process Res. Dev. 13 (2009) 991–998.
[18] F. Studt, F. Abild-Pedersen, T. Bligaard, R.Z. Sørensen, C.H. Christensen, J.K. Nørskov, Science 320 (2008) 1320–1322.
[19] R. Nesper, Angew. Chem. Int. Ed. Engl. 30 (1991) 789–817.
[20] M. Armbrüster, K. Kovnir, M. Behrens, D. Teschner, Y. Grin, R. Schlögl, J. Am. Chem. Soc. 132 (2010) 14745–14747.
[21] G. Wowsnick, D. Teschner, M. Armbrüster, I. Kasatkin, F. Girgsdies, Y. Grin, R. Schlögl, M. Behrens, J. Catal. 309 (2014) 221–230.
[22] R. Ohnishi, W.-L. Wang, M. Ichikawa, Appl. Catal. A: Gen. 113 (1994) 29–41.
[23] Y. Sano, H. Satoh, M. Chiba, M. Okamoto, K. Serizawa, H. Nakashima, K. Omae, J. Occup. Health 47 (2005) 293–298.
[24] A. Ku, O. Oetinscitan, J.-D. Saphores, A. Shapirod, J.M. Schoenunp, Polyhedron 18 (2003) 989–994.
[25] B. Bradley, M. Singleton, A.L. Wan Po, J. Clin. Pharm. Ther. 14 (1989) 423–441.
[26] T. Komatsu, K. Inaba, T. Uezono, A. Onda, T. Yashima, Appl. Catal. A: Gen. 251 (2003) 315–326.
[27] T. Miyake, T. Asakawa, Appl. Catal. A: Gen. 280 (2005) 47–53.
[28] S. Karski, I. Witońska, J. Mol. Catal. A: Chem. 191 (2003) 87–92.
[29] S. Karski, T. Paryjczak, I. Witonñska, Kinet. Catal. 44 (2003) 678–682.
[30] M. Wenkin, P. Ruiz, B. Delmon, M. Devillers, J. Mol. Catal. A: Chem. 180 (2002) 141–159.
[31] I.A. Witońska, M.J. Walock, P. Dziugan, S. Karski, A.V. Stanishevsky, Appl. Surf. Sci. 273 (2013) 330–342.
[32] F.A. Al-Odail, A. Anastasopoulos, B.E. Hayden, Top. Catal. 54 (2011) 77–82.
[33] I. Witońska, A. Królak, S. Karski, J. Mol. Catal. A: Chem. 331 (2010) 21–28.
[34] J.A. Anderson, J. Mellor, R.K.P.K. Wells, J. Catal. 261 (2009) 208–216.
[35] J. Sá, J. Montero, E. Duncan, J.A. Anderson, Appl. Catal. B: Environ. 73 (2007) 98–105.
[36] V. Hessel, G. Cravotto, P. Fitzpatrick, B.S. Patil, J. Lang, W. Bonrath, Chem. Eng. Process. Process Intensif. 71 (2013) 19–30.
[37] W. Bonrath, M. Eggersdorfer, T. Netscher, Catal. Today 121 (2007) 45–57.
[38] R.R.E. Cable, R.E.R. Schaak, R.V. September, V. Re, M. Recei, V. October, Chem. Mater. 17 (2005) 6835–6841.
[39] M.A. Vannice, Kinetics of Catalytic Reactions, Springer Science+Business Media, New York, 2005.
[40] U.K. Singh, M.A. Vannice, J. Catal. 191 (2000) 165–180.
[41] D. Duca, L.F. Liotta, G. Deganello, J. Catal. 154 (1995) 69–79.
[42] G.A. Watson (Ed.), Numerical Analysis, Springer Berlin, Heidelberg, 1978.
[43] J. Wolberg, Data Analysis Using the Method of Least Squares, Springer-Verlag, Berlin, 2006.
[44] J.S. Alper, R.I. Gelb, J. Phys. Chem. 94 (1990) 4747–4751.
[45] A. Borodziński, G.C. Bond, Catal. Rev. 50 (2008) 379–469.
[46] D. Mei, P. Sheth, M. Neurock, C. Smith, J. Catal. 242 (2006) 1–15.
[47] E. Karakhanov, A. Maximov, Y. Kardasheva, V. Semernina, A. Zolotukhina, A. Ivanov, G. Abbott, E. Rosenberg, V. Vinokurov, ACS Appl. Mater. Interfaces 6 (2014) 8807–8816.
[48] Á. Mastalir, Z. Király, G. Szöllösi, M. Bartók, Appl. Catal. A: Gen. 213 (2001) 133–140.
[49] F. Liguori, P. Barbaro, J. Catal. 311 (2014) 212–220.
[50] J.A. Bennett, G.A. Attard, K. Deplanche, M. Casadesus, S.E. Huxter, L.E. Macaskie, J. Wood, ACS Catal. 2 (2012) 504–511.
[51] G.A. Attard, J.A. Bennett, I. Mikheenko, P. Jenkins, S. Guan, L.E. Macaskie, J. Wood, A.J. Wain, Faraday Discuss. 162 (2013) 57–75.
[52] E. Herrero, V. Climent, J.M. Feliu, Electrochem. Commun. 2 (2000) 636–640.
[53] M. Crespo-Quesada, A. Yarulin, M. Jin, Y. Xia, L. Kiwi-Minsker, J. Am. Chem. Soc. 133 (2011) 12787–12794.
[54] A. Ota, M. Armbrüster, M. Behrens, D. Rosenthal, M. Friedrich, I. Kasatkin, F. Girgsdies, W. Zhang, R. Wagner, R. Schlögl, J. Phys. Chem. C 115 (2011) 1368–1374.
[55] H. Okamoto, J. Phase Equilib. 15 (1994) 191–194.
[56] J. Vrest'al, J. Pinkas, A. Watson, A. Scott, J. Houserova, A. Kroupa, Comput. Coupling Phase Diagr. Thermochem. 30 (2006) 14–17.
[57] J. Brasier, W. Hume-Rothery, J. Less-Common Met. 1 (1959) 157–164.
[58] M. Heise, J.-H. Chang, R. Schönemann, T. Herrmannsdörfer, J. Wosnitza, M. Ruck, Chem. Mater. (2014) (Article AS).
[59] R.E. Cable, R.E. Schaak, J. Am. Chem. Soc. 128 (2006) 9588–9589.
[60] J. Gislason, W. Xia, H. Sellers, J. Phys. Chem. A 106 (2002) 767–774.
[61] J. Kitchin, J. Nørskov, M. Barteau, J. Chen, Phys. Rev. Lett. 93 (2004) 156801.
[62] J.A. Rodriguez, D.W. Goodman, J. Phys. Chem. 95 (1991) 4196–4206.
[63] D. Teschner, J. Borsodi, Z. Kis, L. Szentmiklóisi, Z. Révay, A. Knop-Gericke, R. Schlögl, D. Torres, P. Sautet, J. Phys. Chem. C 114 (2010) 2293–2299.
[64] D. Teschner, J. Borsodi, A. Wootsch, Z. Révay, M. Hävecker, A. Knop-Gericke, S.D. Jackson, R. Schlögl, Science 320 (2008) 86–89.
[65] P.W. Albers, K. Möbus, C.D. Frost, S.F. Parker, J. Phys. Chem. C 115 (2011) 24485–24493.